Use of images to model off-axis forces in an electric armour array

J.K. Sykulski, A.A. Roy, K.F. Goddard, D. Swatton and J. Brown

Abstract: The paper describes an investigation into methods of modelling magnetic fields in electric armour arrays. The investigation focuses on large-scale fields, which are responsible for generating off-axis forces, whereas pinch forces produced by localised high flux densities are not considered here. The limitations of 2D modelling are investigated.

1 Introduction

A shaped charge jet is an explosively formed projectile designed to penetrate armour. The penetrative power of these weapons is due to the high speed and small projected area of the jet. To defend against such weapons, an electric armour array may be placed outside the conventional armour. This operates by passing a large current down the length of the jet. The resulting magnetic forces disrupt the jet and thereby increase its projected area. Damage to the conventional armour is therefore spread over a larger area, which reduces the penetrative power of the jet.

There are two types of disruption: one due to pinch forces and the other due to off-axis forces. The pinch forces are due to the axisymmetric field of the current in the jet and squeeze the thin parts of the jet more than the thick parts. The thick parts of the jet are therefore driven outwards, continuing to expand after the current is removed. (Similar work involving pinch forces is described by Hollandsworth [1] which deals with the explosion of segmented wires. Powell [2] has studied the current flow between the small segments of metal which are produced in the explosion.) While the pinch force is probably the main disruption mechanism, if the field of the supply currents is not axisymmetric, off-axis forces occur that may also be important. These off-axis forces cause the point of impact on the conventional armour to vary as a function of the current and the speed and cross-sectional area of the jet. In the following analysis, we will ignore the effects of the disruption on the forces. This allows the jet current to be modelled by a straight current filament.

2 Simplifying the problem

The only practical way to provide currents large enough to disrupt the jet is to use a high-energy capacitor bank — similar to that described in [1]. The current is transferred to and from the jet via a pair of metal plates. These are connected to the capacitor by a pair of thin conducting strips, which are placed close together to provide a low-impedance connection. Where the distance between these strips is small, their currents have little effect on the field in the surrounding air. These portions of the supply strips may therefore be removed, leaving only those parts where the supply strips diverge to meet the plates as indicated in Fig. 1.

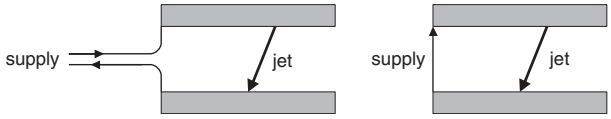

Fig. 1 *Approximate representation of the supply conductors*

Neglecting the thickness (but not the thickness–conductivity product) of this conducting strip gives the simplified model shown in Fig. 2. It can be seen that there are 13 interface surfaces, each of which has finite extent in two directions. Before the method of images can be applied to this problem, further simplification is required. The following three assumptions have been identified which could be used to simplify the model.

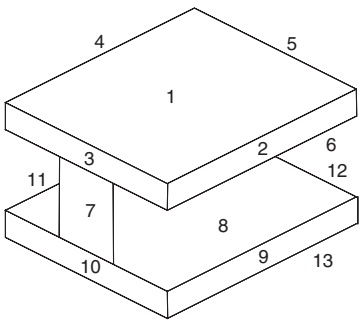

Fig. 2 *The electric armour array showing the 12 faces of the plates and one face representing the supply conductor*

It could be assumed that:

(i) The plates and/or the supply conductor are infinitely conducting. This is good approximation since the frequency of the current is high.

(ii) The width of the supply conductor is equal to the length of the supplied edge of the plate.

(iii) The length and width of the plates are infinite.

IEE Proceedings online no. 20040040

doi:10.1049/ip-smt:20040040

Paper received 11th November 2003.
Originally published online: 19th February 2004

J.K. Sykulski, A.A. Roy and K.F. Goddard are with the School of Electronics and Computer Science, University of Southampton, Southampton SO17 1BJ, UK

D. Swatton and J. Brown are with the Dstl, Fort Halstead, Sevenoaks, Kent TN14 TBP, UK

If all three assumptions are made, the three infinitely conducting surfaces (the supply conductor and the inner faces of the two plates) may be replaced by images of the jet current and of the images used to represent the other surfaces. As explained in Appendix 2 (Section 12.2), these images cancel the normal component of B on the conducting surfaces.

Further simplification can be achieved by assuming that the jet is normal to the surface of the plates. Putting all the images together with the jet current itself, we find that the model consists only of two infinitely long parallel current filaments, as shown in Fig. 3, and is therefore entirely two-dimensional. The two currents flow in opposite directions, and the distance between them is twice the distance between the jet and the supply plane. The force per unit length on the jet is given by $F = 10^{-7} I^2/d$ where I is the jet current and d is the distance between the jet and the supply plane.

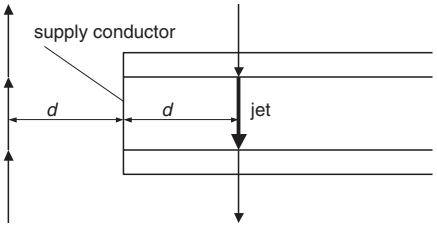

Fig. 3 *The jet current and its images*

While this gives a simple solution, it is of little use in the design process, since most of the parameters of interest have been eliminated from the model. We must therefore consider relaxing one or more of the above conditions.

If the jet enters the plates at an oblique angle, the image currents are also inclined at an angle and cannot be combined into a pair of simple current filaments as described above. In Section 7 it will be shown that the number of filaments needed in the model is not unreasonably large.

3 Finite plates

We now consider the use of images to represent the open edges of the array. If plates with finite dimensions are to be modelled, the field outside the array is linked to the field inside the array. In principle, this would lead to the full three-dimensional model shown in Fig. 2. However, since eddy currents in the plates tend to exclude flux from the interior of the plates, the interaction between the field outside the array and that between the plates is largely confined to the edges of the array. If a boundary condition can be defined to represent each edge of the array, the model can be restricted to the space between the plates. To represent the fringing field at the edges of the array, we can use an infinitely permeable boundary displaced away from the edge of the array. This approximation is illustrated in Fig. 4. The errors associated with this approximation are investigated in Section 4.

Since infinitely permeable boundaries can be modelled using the method of images, it is possible to obtain a semi-analytical solution. The position and sign of the images can be used to compute the magnitude and direction of the off-axis forces on the jet. Though this approach may be implemented irrespective of the angle of incidence of the jet, a simpler solution is obtained if the jet is normal to the plate. This particular case, in which only condition (iii) is relaxed, is described in Section 5.

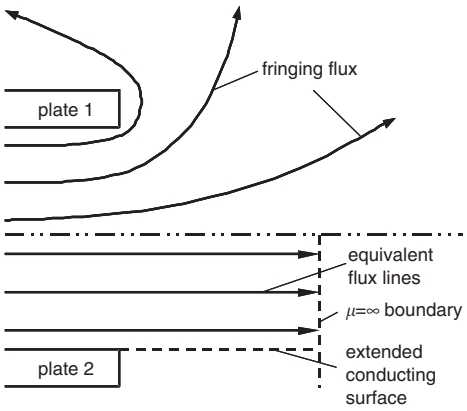

Fig. 4 *Use of displaced boundaries to represent fringing flux*

4 Errors caused by using a displaced boundary

It is intended to allow for flux fringing out around the edges of the plates, by extending the plates to meet an infinitely permeable boundary at some distance beyond the real edges of the plates as shown in Fig. 4. It is therefore appropriate to assess the errors that may be caused by such an approximation. The use of a three-dimensional model to evaluate these errors is not practical, since a very large model is required which would take a long time to run and this would need to be repeated for a large number of cases. Since we can represent the variation in the magnetic field along the edges of the array by Fourier series, an alternative would be to use a number of two-dimensional finite-element models to model the Fourier components of the field. In these models, it is assumed that the scalar potential Ω has the form

$$\Omega = f(x, y) \sin(az) \tag{1}$$

where z is parallel to the edges of the plates, y is normal to the plate surfaces and a is the spatial frequency. Substituting (1) into Laplace's equation gives

$$\frac{\partial^2 \Omega}{\partial x^2} + \frac{\partial^2 \Omega}{\partial y^2} = a^2 \Omega \tag{2}$$

In practice, the limitations of commercial electromagnetic finite-element packages mean that it is often necessary to solve an analogous problem – see Appendix 1 (Section 12.1).

Figure 5 shows the region included in the finite-element models. The surfaces of the conducting plates and the symmetry planes are represented by boundary conditions – only the shaded region is included in the model. The top and right-hand edges of the model are extended beyond the positions indicated in Fig. 5 so that they have no significant effect on the results. The short boundary, which extends from the central plane to the upper plate, has a fixed value of potential imposed to act as the source of the field. The finite-element package solves (2) to give the function $f(x,y)$ in (1). The normal derivative of the potential is then

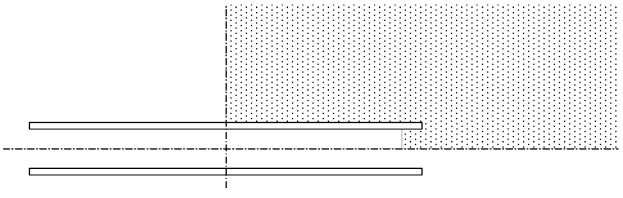

Fig. 5 *Extent of the finite-element models used to model flux fringing around the edges of the plates*

averaged along the same boundary. The ratio of the imposed potential, to its normal derivative is used to calculate the strength of the image field required to represent the edge of the array at the spatial frequency of the model.

If the jet is normal to the plates and the edges of the array are represented by displaced boundaries (as indicated in Fig. 6), Ω is independent of y and the solution to (2) becomes

$$\Omega = Ke^{-ax} - be^{ax} \tag{3}$$

where K and b are constants. The first term represents the field due to the jet current and its images reflected in the other boundaries of the array, while the second term represents the field of the images reflected in the edge being modelled. Since $\Omega = 0$ at the infinitely permeable boundary,

$$b = K\exp(-2a(X + d)) \tag{4}$$

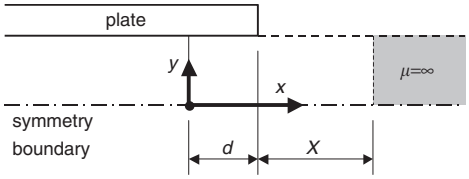

Fig. 6 *Position of plate edges and equivalent boundary*

To estimate the errors caused by the use of the displaced boundary, this value of b should be compared with one obtained from the finite element model. Differentiating Ω in (3) gives

$$H_x = -\frac{\partial \Omega}{\partial x} = a(Ke^{-ax} + be^{ax})$$

Hence

$$\frac{H_x}{\Omega}_{|x=0} = a\left(\frac{K+b}{K-b}\right)$$

Denoting the ratio H_x/Ω at $x = 0$ by γ we find that

$$b = K\left(\frac{a-\gamma}{a+\gamma}\right) \tag{5}$$

The difference between the strength of the reflected field calculated from the finite-element model and that calculated for a reflecting boundary at various distances beyond the edges of the real plates has been plotted as a function of the spatial frequency a (see Fig. 7). Note that this difference represents the error as a percentage of the source field, not of the image field. The results in Fig. 7 were obtained for a plate of width 1m, thickness 10 mm and separation 100 mm.

At low spatial frequencies, the error tends to zero when $X = 89.9$ mm. This value of X could be calculated from the inductance per unit length of current flowing in the two plates. For higher spatial frequencies, the optimum value of

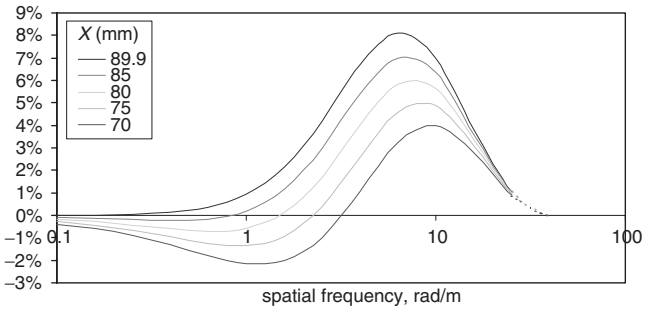

Fig. 7 *Errors when $d = 50$ mm as a percentage of the source field*

X is lower. The value of d in the finite element model was set to half the plate separation, i.e. 50 mm, to allow the field to be reasonably uniform at $x = 0$. If the position of the reflecting boundary is set for zero spatial frequency, the maximum error 50 mm in from the plate edges would be about 8% of the source field and would occur for a spatial frequency of around 6.5 rad/m. Equation (3) suggests that the errors vary in proportion to $\exp(-2ad)$; consequently, the errors for high-spatial-frequency components are greatly reduced for larger values of d.

5 Solution to the two-dimensional approximation

Using the displaced-boundary model of the array edges discussed above, the method of images can easily be applied to the case of finite plates, provided that the jet is normal to the plate surfaces and the width of the supply conductor is equal to that of the plates. In this case, images need to be considered in all four sides of the plates.

Images of the jet current are produced by reflection in the boundaries of the modelled air space. The z component of current is unchanged when the current is reflected about the plate surfaces or the displaced boundaries representing the unconnected edges of the array, but is reversed when the current is reflected about the supply conductor.

Fig. 8 illustrates the arrangement of currents used in the image-based models. The symbols $\oplus$ and $\odot$ represent currents flowing into and out of the page, respectively. The solid rectangle represents the plates and encloses the jet current, while the broken lines represent the boundaries of the modelled space and its images reflected in these boundaries. The signs of the image currents have been chosen to represent the case where the whole of the left-hand side of the array is connected to the supply. In principle, there should be an infinite array of images; the calculations therefore used a larger 18×26 array.

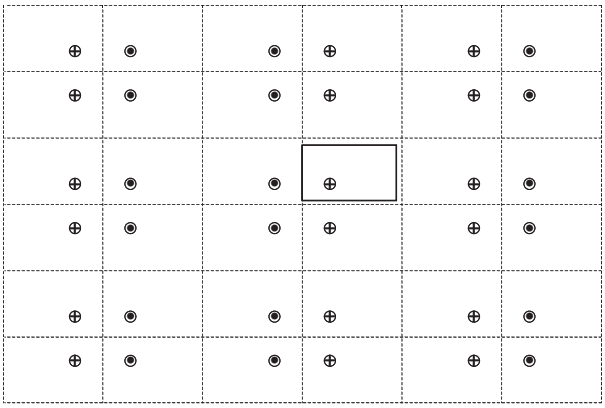

Fig. 8 *Position and sign of the image currents*

Note that, to avoid gross errors, it is necessary to ensure that the total current flowing to the right of the supplied edge of the plate is correct. For simplicity, this condition was enforced by always having an odd number of rows to the left and right of the supply plane.

The force F due to each image current is given by

$$F = \mu_0 I^2/(2\pi R_{image-jet})$$

where $R_{image-jet}$ is the distance between the jet and the image. The inductance per unit length (plate spacing) is calculated as follows. The vector potential A_z due to the field of any one image is given by

$$A_z = (\mu_0/2\pi)I_{image}\ \ln(R_{image-ref}/R_{image-jet})$$

where $R_{image-ref}$ is the distance between the image and the reference point on the supplied edge of the plate. The vector potential A_z due to the jet current itself is given by

$$A_z = (\mu_0/2\pi) I_{jet} \ \ln(R_{jet-ref}/R_{jet})$$

where $R_{jet-ref}$ is the distance from the centre of the jet to the reference point and R_{jet} is the radius of the jet. It is assumed that the jet current is uniformly distributed over the cylindrical surface of the jet, while flux linkage and flux density are calculated on the central axis of the jet. From Fig. 5 it is clear that, for each image current, there is another image (or the jet itself) which is the same distance from the reference point and which carries the opposite current. When the fluxes due to these two currents are added together, the $\ln(R_{image-ref})$ terms all cancel out. Hence the inductance L per unit length (plate spacing) is given by

$$L = \frac{\mu_0}{2\pi}\left(-\ln(R_{jet}) - \sum_{images} \frac{I_{image} \ln(R_{image-jet})}{I_{jet}}\right)$$

As a means of checking the calculation, the forces and inductances obtained from the method of images were compared with results obtained from finite-element analysis. The two sets of results were found to be in good agreement. The maximum error was less than 3.5%, occurring when the jet was farthest from the powered edge of the plates.

Figure 9 shows the magnitude and direction of the total off-axis force in proportion to the stored magnetic energy $I^2L/2$. Relating the force to the stored magnetic energy is appropriate, since most of the energy stored in the capacitor will be converted to magnetic energy; hence, while the peak current will vary as a function of the inductance, the peak magnetic energy varies much less. Comparison with the values for semi-infinite plates (also shown in Fig. 9) indicates that the unconnected edges of the plates increase the forces. This effect is greatest when the jet is near to the unconnected edges.

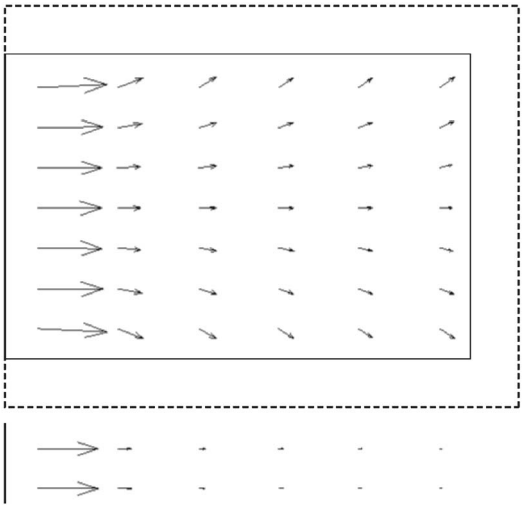

Fig. 9 *Effects of finite plate size on off-axis forces*
Arrows in the lower figure indicate values for semi-infinite plates

Figure 10 shows the surface current density predicted by a two-dimensional finite-element model. The solid rectangle represents one plate, while the broken-line rectangle shows the boundary of the extended plates. In reality, the currents shown outside the solid rectangle do not flow in the positions indicated, but instead flow on the edge faces of the plate or close to the edges on the outer faces of the plates.

The losses in the plates may be estimated from the surface current density, but it must be accepted that the losses due to surface currents flowing close to the edges of the plates will be higher than predicted. However, since the bulk of the losses occur in or close to the jet or the supply conductor, the overall error will be small.

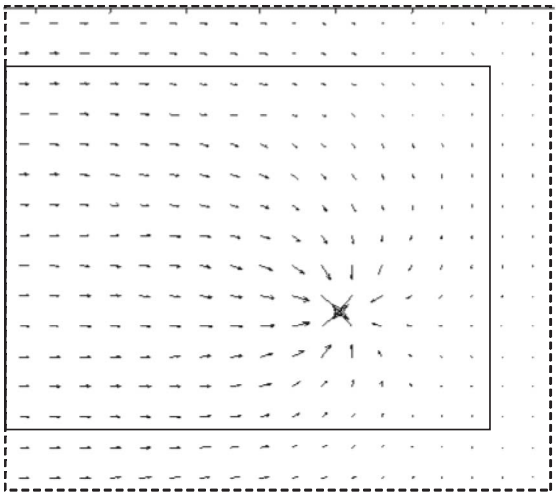

Fig. 10 *Plot showing the surface current density on the extended plates*

6 Supply conductors of finite width

If the width of the supply conductor is no longer equal to that of the supplied edges of the plates, images cannot be used to represent the supply conductor. In this case, it is necessary to model the supply conductor explicitly and to represent the supplied edges of the plates by a displaced boundary in the same way as for the unsupplied edges of the array. This makes the method of images more difficult to implement for two principal reasons. First, it is more difficult to calculate the field of a current sheet than that of a filamentary current. Secondly, the distribution of the current in the supply conductor is unknown.

For the case when the jet is normal to the plates, an alternative approach is available using two-dimensional finite-element analysis. This method allows both the finite width and the finite conductivity of the supply conductor to be modelled. Accurate modelling of the eddy currents in the supply conductor would require the use of a transient model. However, owing to the high frequency of the current, the flux penetrating the supply conductor is small. Consequently the errors introduced by using a steady-state AC model will also be small.

The results presented in Fig 11 were obtained using a series of steady-state AC finite-element models. The co-ordinate axes are chosen so that x and y lie in the plane of the plates and the current flows normal to the plates, in the z direction. The off-axis force on the jet is then given by

$$F = (-IB_y, IB_x, 0)$$

Since I and B both vary sinusoidally with angular frequency ω, the products IB_y and IB_x will consist of the sum of two terms: a constant term and an oscillatory term with angular frequency 2ω. When these terms are averaged with respect to time over one cycle, the oscillatory term contributes nothing. The average component of the force is therefore obtained from the constant term. The average force in proportion to the stored magnetic energy is obtained by dividing by $I^2L/2$. These forces are shown in Fig. 11. It is useful to compare Fig. 11 with Fig. 9. Notice that a supply conductor of finite width tends to reduce the off-axis forces on the jet.

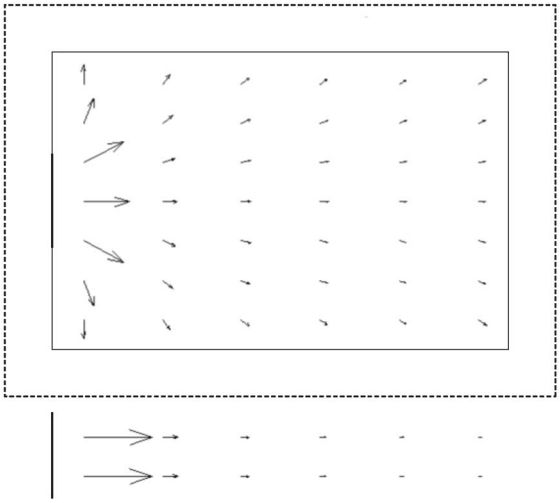

Fig. 11 *Off-axis force on the jet as a function of position*
Top: with finite plates and supply conductor represented by the bold-line segment. Broken line represents the displaced boundary
Bottom: with infinite supply conductor and plates

In Section 8, a method is described which uses an image-based model to estimate the errors caused by using the two-dimensional approximation for other angles of incidence, as indicated in Fig. 12. Using these estimates, the values calculated by the finite-element model can be adjusted to improve their accuracy. Although approximate, this method is simple to use and draws upon the strengths of both finite-element and image based methods.

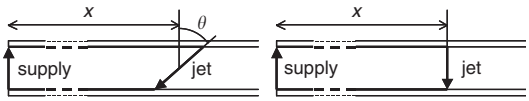

Fig. 12 *Approximate representation of an inclined strike*

7 Inclined jets

This Section deals with the case in which the plates and supply conductor are infinite and the jet enters the array at an oblique angle. Since the plates are infinitely conducting, the B_z component on the surface of the plates is zero. The B_z component of the real current filament at the surface of the upper plate may be cancelled by adding an appropriate image current. A similar image current will cancel the B_z component on the lower plate. Consequently, further image currents are required to cancel these secondary fields. In principle, this leads to an infinite series of images. It is therefore necessary to truncate the series or, as in Fig. 13, to replace the distant zig-zag line segments by a straight line. Figure 13 also shows a further set of image currents, which represents the effect of the supply connection. It is assumed that eddy currents in the supply conductor will eliminate the normal component of B. The second set of images ensures that the normal component of B is zero. The magnitude of H produced by a single image current I is given by

$$H = \frac{I}{4\pi R}(\cos\theta_1 - \cos\theta_2)$$

where the dimensions are as illustrated in Fig. 14. This equation is applied to each filament in the zig-zag series in Fig. 13. A program has been written to calculate the total field at any point. The program uses four input variables to define the position of the jet in relation to the supply conductor. These are described in Fig. 15.

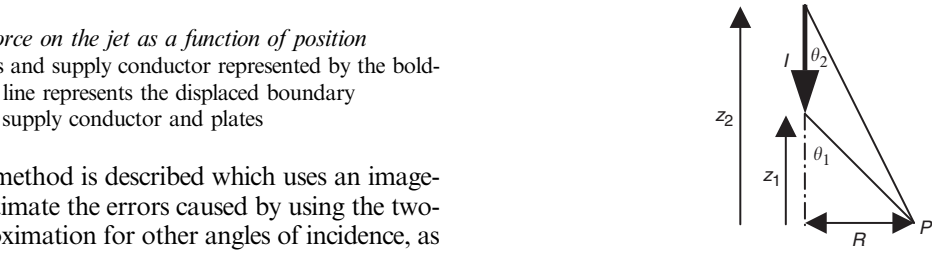

Fig. 13 *The jet current and its images*

Fig. 14 *The current filament I showing the variables used in the calculation of H and A*

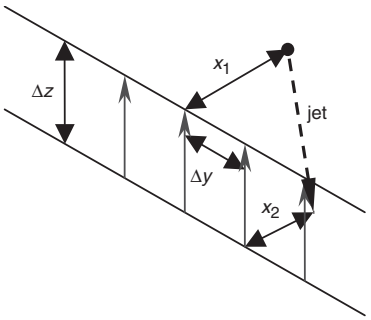

Fig. 15 *Position of jet in relation to the supplied edge of the array*

To obtain the force on the jet we need to evaluate the field at a number of points along the jet. Since the field of the jet current would be infinite at these points, the contribution of this current filament must be omitted from the calculations. This field produces no net force since it is axisymmetric. At one end of the jet, the nearest image filament would also produce an infinite field. This infinity could be avoided by replacing this filament by a current sheet that carried the same total current. However, this would make the calculations more difficult and would not model the true situation where the jet penetrates the plate. We therefore chose to avoid evaluating the field very close to the ends of the jet.

Figure 16 shows the surface current density on the upper and lower plates in the case when $x_1 = 0.6$, $x_2 = 1.1$, $\Delta y = 0$ and $\Delta z = 0.5$, i.e. the jet enters the plates at an angle of 45°. This is calculated from the H field using $J_s = H \times n$ where n is the unit vector normal to the surface of the plate. Note that, although the current is fed into the top plate from the left, the bulk of the current enters the jet from the right. This is because the jet and its first image are closer on this side and produce a stronger field.

To obtain the inductance, we require to evaluate the vector potential A due to the jet and all its images. The

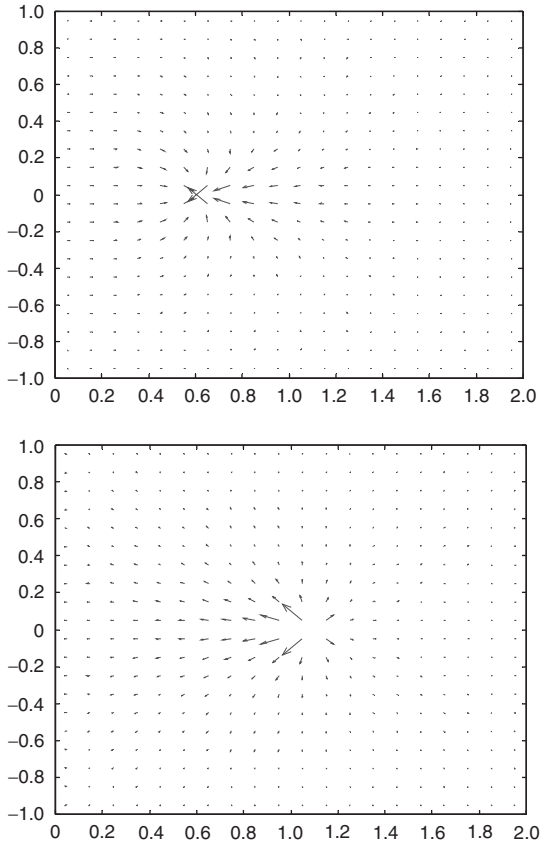

Fig. 16 *Plots showing the field of J_s on the upper and lower plates*

magnitude of A produced by a single image current I is given by

$$A = \frac{\mu_0 I}{4\pi}\int_{z_1}^{z_2}\frac{dz}{\sqrt{(R^2+z^2)}} = \frac{\mu_0 I}{4\pi}\ln\left(\frac{z_2+\sqrt{(z_2^2+R^2)}}{z_1+\sqrt{(z_1^2+R^2)}}\right) \quad (6)$$

where the dimensions are as illustrated in Fig. 14. The direction of A is the same as that of the current. When $R=0$ and z_1 and z_2 have opposite signs a singularity occurs. Hence, the contribution of the jet current itself must be calculated with $R = R_{jet}$.

8 Local effects of inclining the jet

The results in Sections 5 and 6 assume that the jet is normal to the plates, and are only approximately true when the jet enters at angle θ, to the normal. In the case of an oblique entry, a torque acts on the jet and the inductance of the circuit increases. These effects are local and do not involve the supply conductor or the edges of the array. In this Section, a method is described using simplified three-dimensional models to estimate this torque and the increase in inductance.

Consider the jet current and the first few images reflected in each conducting plate, as shown in Fig. 17. This model, which ignores the B field due to the supply conductor and the array edges, can be used to investigate the effect of an inclined jet on the torque and inductance. Since the current appears and disappears at the ends of the chain of current filaments, it is not a complete model. This suggests that current flows through empty space, to and from the free ends of the filaments. The model could be completed by adding a pair of current filaments on the z axis to extend the chain to infinity, but this would result in infinite inductance.

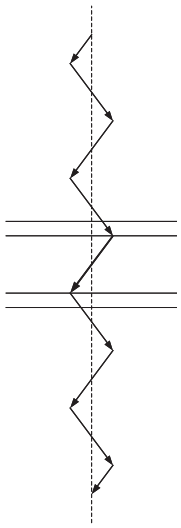

Fig. 17 *The jet and its images*

It is therefore necessary to use the incomplete model. Appendix 3 (Section 12.3) discusses the errors caused by using such incomplete models.

The force at any point on the jet is obtained by computing the B field due to all the images and taking the cross product with J. If the ratio of the jet radius to the plate spacing is constant, the torque T is proportional to the plate spacing s, to I^2 and to a function of the angle of incidence θ.

A substantial proportion of this torque is generated within a few jet radii of the ends of the jet. Inaccuracies occur when computing the torque in this region due to the singularities in the B field. These occur at the point where the jet current meets its image. The singularity could be avoided by replacing the filament by a current sheet as suggested in Section 7. However, this effort is not justifiable since in reality a hole exists between the jet and plate. This hole allows flux to escape, reducing the force.

Figure 18 shows $T/(sI^2)$ as a function of θ. The force was evaluated at 25 points along the length of the jet and the torque was obtained using the mid-ordinate rule.

Fig. 18 *The effect of varying the angle of incidence on the torque*

In addition to this torque, inclining the jet has two other significant effects; the inductance of the circuit is increased, and there is an additional force component normal to the plate surfaces. The z component of force can be calculated from the x and y components of force using

$$F_z = -\left(F_x(x_2-x_1)+F_y\Delta y\right)/\Delta z$$

where the dimensions are as indicated in Fig. 15. The values of F_x and F_y are found, to first order, using the two-dimensional models described in Sections 5 and 6.

The increase in inductance was calculated by comparing $\int A\,\mathrm{d}l$ [calculated using (6)] for the inclined jet with that for $\theta = 0$, and is plotted in Fig. 19.

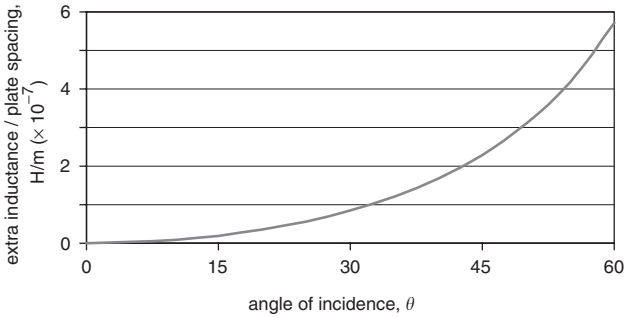

Fig. 19 *Increase in inductance due to inclining the jet*

9 Conclusions

Given certain simplifying assumptions, it is possible to obtain the off-axis forces on the jet using either the method of images or two-dimensional finite-element analysis. The method of images, in particular, offers a very efficient way of computing the off-axis forces.

A difficult case to model using either method occurs when the jet enters the plates at an inclined angle and when the supply conductor has finite width. In principle, this case could be solved using three-dimensional finite-element analysis but this requires the use of more sophisticated software and significantly longer computing times.

10 Acknowledgment

The authors gratefully acknowledge the support of the UK Ministry of Defence in the form of the funding from the Corporate Research Programme, package TG06.

11 References

1 Hollandsworth, C.E., Powell, J.D., Keele, M.J., and Hummer, C.R.: 'Electrical conduction in exploded segmented wires', *J. Appl. Phys.*, 1998, **84**, (9)
2 Powell, J.D., Thornhill, L.D., Batteh, J.H., and Verdon, M.: 'Current distribution and resistance characteristics in plasma injectors for electro-thermal-chemical launch', *IEEE Trans. Magn.*, 1999, **35**, (1) pp. 218–223
3 Hammond, P.: 'Electric and magnetic images' *IEE* Monograph 379 1960

12 Appendixes

12.1 Appendix 1

If the scalar magnetic potential is as described in (1), the Laplace equation given by (2) may be solved using the following analogue problem. Instead of a static scalar magnetic-potential solution with cos *az* variation, the analogue problem uses a two-dimensional transient eddy-current solution in vector potential with $\exp(\alpha t)$ variation. From Maxwell's equations,

$$\nabla \times (\nabla \times A) = \mu J = -\mu\sigma \frac{\partial A}{\partial t}$$

Assuming a two-dimensional solution of the form

$$A = (0, 0, f(x, y)e^{\alpha t})$$

we obtain the equation

$$\frac{\partial^2 A_z}{\partial x^2} + \frac{\partial^2 A_z}{\partial y^2} = \alpha\mu\sigma A_z$$

This partial differential equation is of the same form as that given by (2). The value of α required to obtain the correct distribution of scalar magnetic potential is given by $\mu\sigma\alpha = a^2$.

12.2 Appendix 2

The method of images is based on analogies with the familiar phenomenon caused by the reflection of light in a mirror. The following examples are relevant to the use of images described in this paper.

Consider an isolated conductor carrying a current *I* near to an infinitely permeable boundary of infinite extent as shown in Fig. 20. An equivalent arrangement is obtained by placing an image current beyond the symmetry plane, as indicated. This will cancel the tangential component of *B* on the symmetry line.

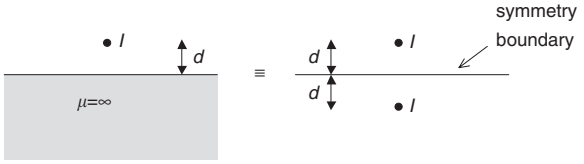

Fig. 20 *Image for an infinitely permeable boundary*

Now suppose that the boundary is infinitely conducting. In this case the normal component of *B* is zero on the symmetry boundary. An equivalent arrangement is shown in Fig. 21.

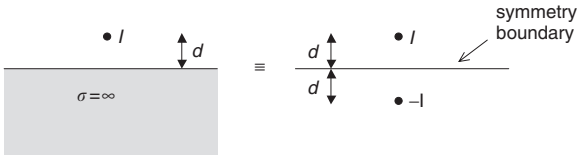

Fig. 21 *Image for an infinitely conducting boundary*

Finally, consider the case of a current filament orientated at some angle to an infinitely conducting boundary. An equivalent arrangement is shown in Fig. 22.

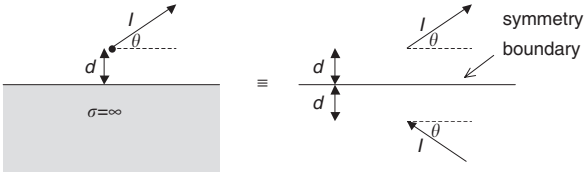

Fig. 22 *Image for an infinitely conducting boundary for current filament oriented at angle θ*

For further explanation on the use of images in electromagnetic theory see [3]. The method of images can also be used when the surface is bounded by infinitely conducting or infinitely permeable surfaces, which meet the surface at 90°.

12.3 Appendix 3

As noted in Section 8, the use of an incomplete model implies that the current flows through empty space to

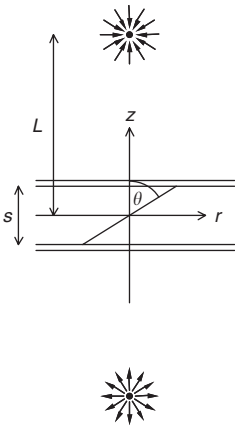

Fig. 23 *Source and sink*

complete the circuit. To estimate the effects of these currents we shall begin by estimating the B fields which they produce in the region of interest.

From Fig. 23, it can be seen that the current density at the origin is given by

$$J = \frac{2I}{4\pi L^2}$$

where I is the current flowing between the source and the sink. Therefore

$$B = \frac{\mu_0 Ir}{4\pi}$$

The difference between the flux linkage for a jet at angle θ and that for $\theta = 0$ is given by

$$\Delta\phi = \int_{-s/2}^{s/2} \int_{0}^{z\tan\theta} B\, dr\, dz = \frac{\mu_0 I\, s^3 \tan^2\theta}{96\pi L^2}.$$

If $L > 4s$ this contributes less than 1% of the change in inductance indicated in Fig. 19. The torque produced by the above B field acting on the jet current is given by

$$T = \frac{\mu_0 I^2 s^3 \tan\theta}{48\pi L^2 \cos^2\theta}$$